Article

Monitoring Coastal Erosion Using Remote Images: Comparison between Physically and Remotely Acquired Data on a Limestone Coast

Joanna Causon Deguara [1,*]**, Ritienne Gauci** [1] **and Rob Inkpen** [2]

[1] Department of Geography, University of Malta, MSD 2080 Msida, Malta
[2] School of Environment, Geography and Geosciences, University of Portsmouth, Portsmouth PO1 2UP, UK
*   Correspondence: joanna.causon-deguara.10@um.edu.mt

Abstract: Boulder-sized clasts on rocky coasts are considered as erosional signatures of extreme wave events and boulder attributes are often used in numerical models to estimate wave characteristics. The use of unmanned aerial vehicle (UAV) technology and related software has facilitated the monitoring of coastal areas, by generating models from which 2D and 3D measurements can be derived. However, the reliability and preciseness of such measurements is still to be determined. This study seeks to analyse the accuracy of boulder measurements by comparing the dimension data obtained through in-situ measurements with ex situ data generated from digital models, based on UAV images. The study area is a bouldered sloping coast located on the southeast coast of Malta (Central Mediterranean) that has developed into multiple limestone dipped strata with a fractured and heavily jointed morphology. The dimensions of c. 200 boulders in different morphological settings, such as clusters or ridges, have been statistically compared. The results show a very strong correlation between the two datasets, both in 2D and 3D; however some notable differences were observed at the individual boulder level. For the majority of boulders analysed, the A and B axes dimensions varied by ±10% to 20%. The C axis proved to be harder to measure accurately and showed a wider range of difference. Boulder volume results in the majority of cases varied from 0% to ±40%. Some tested methods of volume calculation may be more accurate and realistic than others depending on the boulder position in relation to other clasts and shore morphology. An automated digital analysis of the terrain surface to identify the boulder extents may offer possibilities for a more accurate estimation of boulder attributes.

Keywords: coastal boulder deposits; coastal erosion; unmanned aerial vehicles; coastal monitoring; rock coast; Malta

1. Introduction

Coastal boulder deposits (CBDs) identified on rock coasts have been the focus of numerous studies in the last two decades [1]. They are considered to be the product of erosional processes generally associated with extreme wave events, produced by major storms, hurricanes and even tsunamis [2,3]. Understanding the wave climate and frequency of such extreme events is important for assessing the inundation limits and coastal erosion rates, which are essential information for coastal planning and protection. Similarly, the identification of occurrences of extreme waves, such as tsunamis, have implications on coastal hazard assessment [4].

Various numerical models have been proposed to estimate the wave magnitude that is capable of detaching, entraining and transporting these boulders across the backshore and foreshore [5–8]. Such models require the input of boulder data, namely long, intermediate and short axis dimensions, volume and weight. However, collecting boulder data is by no means always an easy task. It is cumbersome, time consuming and labour intensive, often requiring more than one person on the field. Other possible issues include accessibility and

site safety, favourable weather conditions and limited time frames of accessibility due to tidal inundations.

New approaches in geomorphological investigations are currently being introduced in coastal boulder research to enable the identification and monitoring of storm erosion signatures at different spatial and temporal scales. The use of remotely collected data, such as from satellite imagery, has been tried and discussed [9–11]. The successful application of satellite images for boulders' assessment is to some extent limited by the resolution and clarity of these images and it is typically difficult to clearly identify and measure boulders smaller than 1 m [9]. Drones, or unmanned aerial vehicles (UAVs), now offer a fairly inexpensive way to acquire high resolution datasets over extensive areas and hence the possibility of collecting sufficient, representative data from large accumulations [12–15]. Repeated 3D imagery data can be used to identify and map changes in the location of hundreds of mobile and immobile boulders along the coasts and relate the changes to boulder size and elevation [16–19].

The aim of this study is to assess the reliability and accuracy of data obtained remotely, and to assess to what extent it can be used without any level of ground truthing. This was carried out by comparing boulder characteristics measured physically on site to those obtained through a model generated from aerial images. Comparisons are made between the in-situ measured dimensions of the three main boulder axes (A, B, and C) and the volume, as calculated by the geometric formulas using the three main axes with those derived from the 3D model. The volume results from six individual boulders were further validated using structure from motion (SfM) techniques to build a 3D model of each boulder, from which a more precise volume measure was derived. The majority of clasts measured (98%) fall into the boulder category, as defined by [20] with a B axis greater than 0.40 m and less than 4.1 m. Only three clasts out of 198 exceeded the 4.1 m threshold.

2. Study Area

The study area is known as Żonqor Point and is located in the coastal town of Marsascala, in southeast Malta (Figure 1). The coast trends in a northwest-southeast orientation and faces the northeast. The geology of the coast consists of very gently inclined limestone strata that dip towards the sea in a north-easterly direction. Two formations are exposed as outcrop, the Mara member of the Lower Coralline Limestone formation (LCL), which is found at or just below sea level, and the Lower member of the Globigerina Limestone formation (LGL) which overlies the LCL. The LGL can be described as a pale yellow, generally homogenous, fine-grained limestone, composed mainly of Globigerinid foraminifera [21]. The LCL is rather hard, finely textured with a pale cream colour and some rust mottling. The typical fossil content includes large echinoid spines, bryozoans and large foraminifera [21]. The transition between these two lithologies is marked at this location by a phosphatic horizon showing some large and relatively flat nodules. Both formations are of an Oligocene, late Chattian origin > 23.0 Ma.

The outcropping beds are dissected by a conjugate set of joints that mainly run normal to the shoreline and subparallel to it. The boulder production occurs as blocks are detached by wave action generally along the exposed joints and bedding planes, as their aperture gradually widens by subsequent wave impact (Figure 2). Thus, the spacing between joints and bed thickness play an important role in determining the boulder dimensions, although further breakage often occurs with subsequent transportation by waves.

Figure 1. Location of the study area outlined in red. Areas outlined in yellow indicate the presence of salt pans (Source: Google Earth).

The weather across the Maltese Islands is influenced by the movement of air masses that develop over the Atlantic, Eurasia and Africa. Storms usually occur in the autumn and winter seasons and are typically generated by low pressure systems meeting the warm moist air over the Mediterranean [22]. The prevailing wind and wave direction is from the northwest and waves hit this part of the coast obliquely. However, occasional strong north-easterly winds are known to generate high waves from this direction. These waves can be very powerful and destructive also due to the gentle slope of the coast in a north-easterly direction.

Anthropogenic interventions on the coast are evident in the creation of salt pans that have been hewn out of some sections of the surface bedrock (Figure 2).

The boulder deposits observed along various parts of the coast of the Maltese Islands have been studied in recent years [23–27]. The aim of these studies was primarily to identify the event type, storm or tsunami, to which detachment and transportation could be attributed.

Figure 2. Top left: Boulder accumulations on site. **Top right**: Joints and fractures in outcropping bedrock structure. **Bottom**: Salt pans hewn out of bedrock.

3. Materials and Methods

3.1. Data Obtained during Fieldwork

The long, intermediate and short axis dimensions of 432 boulders were measured on site during a series of field studies carried out between October 2013 and October 2014. The data was used for a previous study [23,27], the focus of which was to assess the wave height required for boulder transport. In order to avoid an overestimation of boulder dimensions and volume, when a boulder shape was seen to be somewhat irregular or varying widely from a cuboid shape, the average axis dimensions were taken. Similarly, the volume was calculated according to the geometrical shape of each boulder (e.g., cubic, triangular, spherical, etc.)

For the present study a 3D model was generated from the aerial images obtained from a UAV. The UAV flight was carried out in April 2022. One hundred and ninety-eight of the 432 boulders were subsequently identified in the 3D model with the aid of site photos and were measured from the model.

3.2. Aerial Data Acquisition and 3D Model Generation

The UAV model used to capture the aerial images is an EVO 2 Pro drone (Autel, Germany), which is equipped with a 1″ CMOS 20 MP camera. The flight extended over a stretch of coastline approximately 500 m long and 80 to 100 m wide, covering an area of around 0.04 km^2. The flight path was pre-programmed to run parallel to the coast and was set at an elevation of 30 m with a front overlap of 80% and a side overlap of 70%, as recommended by image processing software Agisoft Metashape (Version 1.8.0) [28]. Similar overlaps have been used in other studies e.g., [16,18]. The importance of adequate and sufficient overlap between images has been emphasized in the literature [29].

　　　　The 3D model was generated from 823 geotagged aerial images. The software used to produce the model is Agisoft Metashape Ver 1.8.0. This software generates 3D models from the photogrammetric processing of aerial images and has been used for coastal studies [16–18,30]. Once the photos were uploaded and aligned, a dense point cloud of over 330 million points was generated. A digital elevation model (DEM) with a resolution of 1.22 cm/pixel and an orthomosaic model with a resolution of 6.22 mm/pixel were subsequently developed (Refer Figure 3).
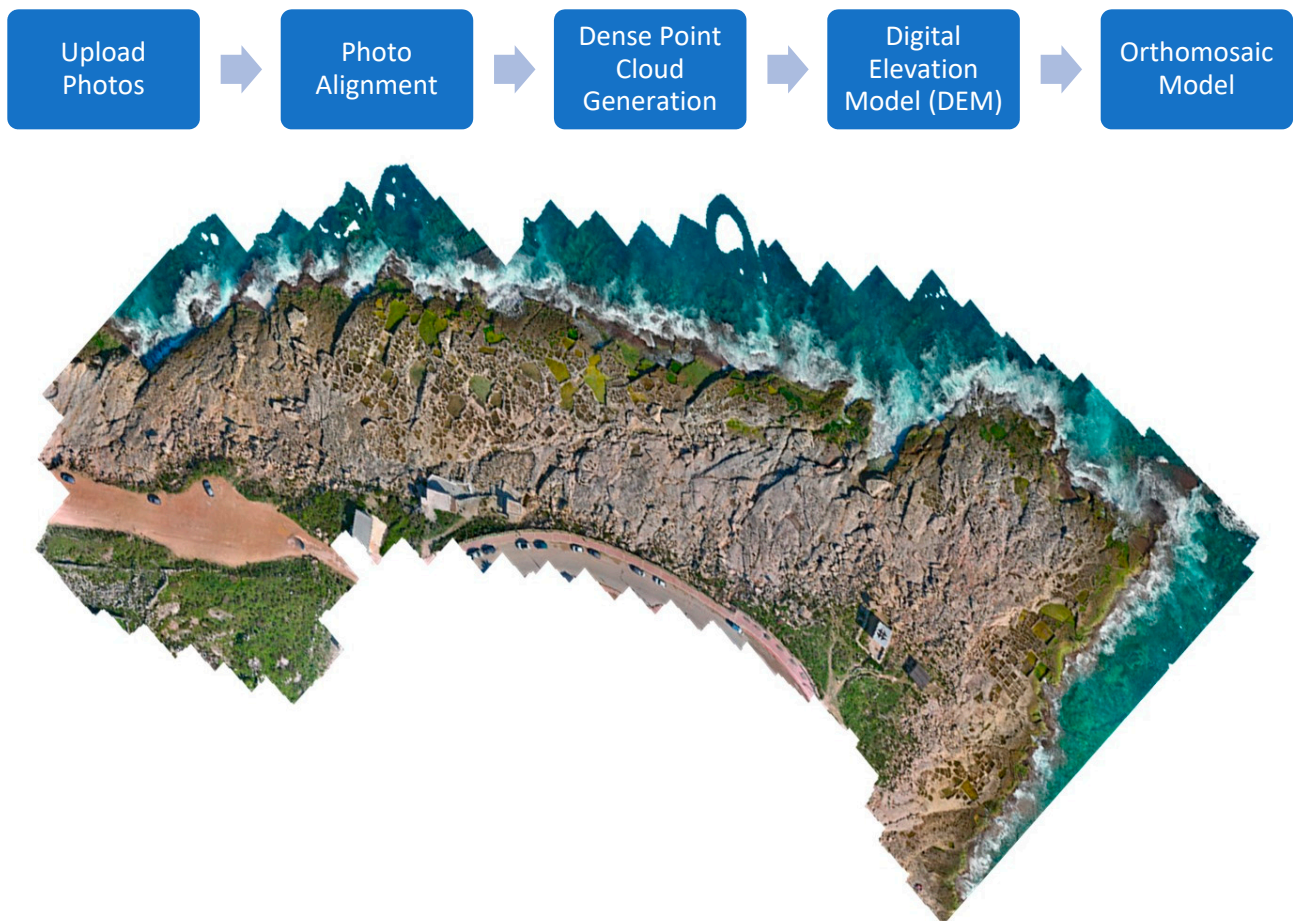

Figure 3. Processing workflow on Agisoft Metashape for the creation of a coastal 3D model (orthomosaic).

3.3. Measurements from the 3D Model

　　　　For the axis dimensions, both the maximum and average boulder A, B and C axes were taken. The maximum dimensions refer to the highest values for the A, B and C axis dimensions, whilst the average dimensions refer to the median dimensions, when taking into consideration the irregularity of the boulder shape (refer Figure 4).

　　　　All measurements derived from the model were taken using Agisoft Metashape software functions. The linear and polyline measurement tools were used to measure the A, B and C axis dimension (Figure 5), whilst the area and volume were measured using the polygon tool to outline each individual boulder to be measured, and the area and volume tool (Figure 6).

　　　　Measuring the A and B axes was relatively unequivocal, as they could be measured directly from the model. The linear dimensions were taken either by using the measuring tool for the flat-lying boulders, or the polyline tool when the boulders were seen to be inclined or imbricated. In order to replicate as best as possible the methods used for the in-situ measurements, both the maximum and average dimensions were taken.

The C axis was the hardest to measure with any degree of certainty as in most cases it was not possible to measure directly due to the location of the boulder relative to its surroundings. In some instances, the C axis was not clearly visible or partially obstructed from view, due to shadows or other surrounding clasts. In such cases, it was measured using the polyline tool and was estimated from the difference between the surface of the boulder and the underlying ground, as shown in Figure 5. This is not always straightforward as often boulders are of an uneven thickness, or the ground level may be irregular due to the slope gradient, surface roughness, or the presence of low scarps. Similar issues were encountered when boulders were found in a cluster or overlying other clasts in a boulder ridge. In most cases, it had to be an educated guess or the average of the highest and lowest values.
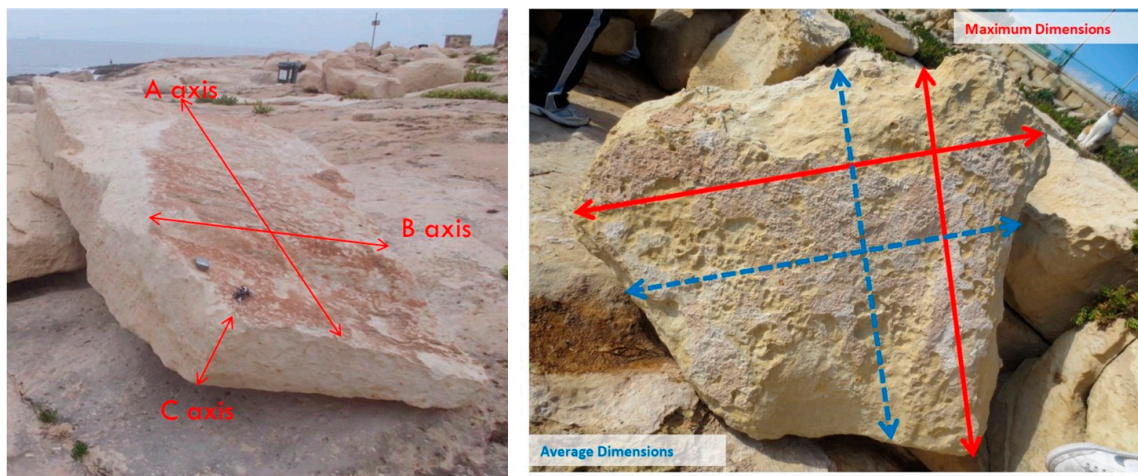

Figure 4. Left: Example of the A (longest), B (intermediate) and C (short) axes. **Right**: Maximum and average dimensions measured for irregularly shaped boulders.

The boulder surface area was measured by drawing a polygon around the edges of the boulder surface using the polygon tool and using the measure shape function to estimate the surface area (Figure 6).

The boulder volume was derived from the collected data as follows:

i.　By applying basic geometric formulas for the volume calculation, according to the boulder shape (e.g., V = l × b × h for cubic boulders, V = 0.5 × l × b × h for triangular boulders) and using the A, B and C axis dimensions acquired:

　○　from the in-situ measurements obtained during field trips;
　○　from the average boulder dimensions obtained from the model;
　○　from the maximum boulder dimensions obtained from the model.

ii.　Calculated using Agisoft Metashape software using the in-built function for the volume calculation with the 'best fit' option and 'custom plane' option. Through the volume calculation facility—by drawing an outline around each boulder—the software calculates the boulder volume from the difference in elevation between each point on the boulder surface and the ground. In the best fit option, the ground level on which the boulder rests is automatically determined by the software from XYZ coordinates of the selected vertices. In the custom plane option, the ground level is determined by the user;

iii.　Calculated by multiplying the boulder surface area by the C axis, as derived from the model. This measurement was used as another option to calculate the volume. Through this method, overestimation of the volume (due to inaccurate A and B axis measurements or due to the imbricated position of the boulder) are avoided.
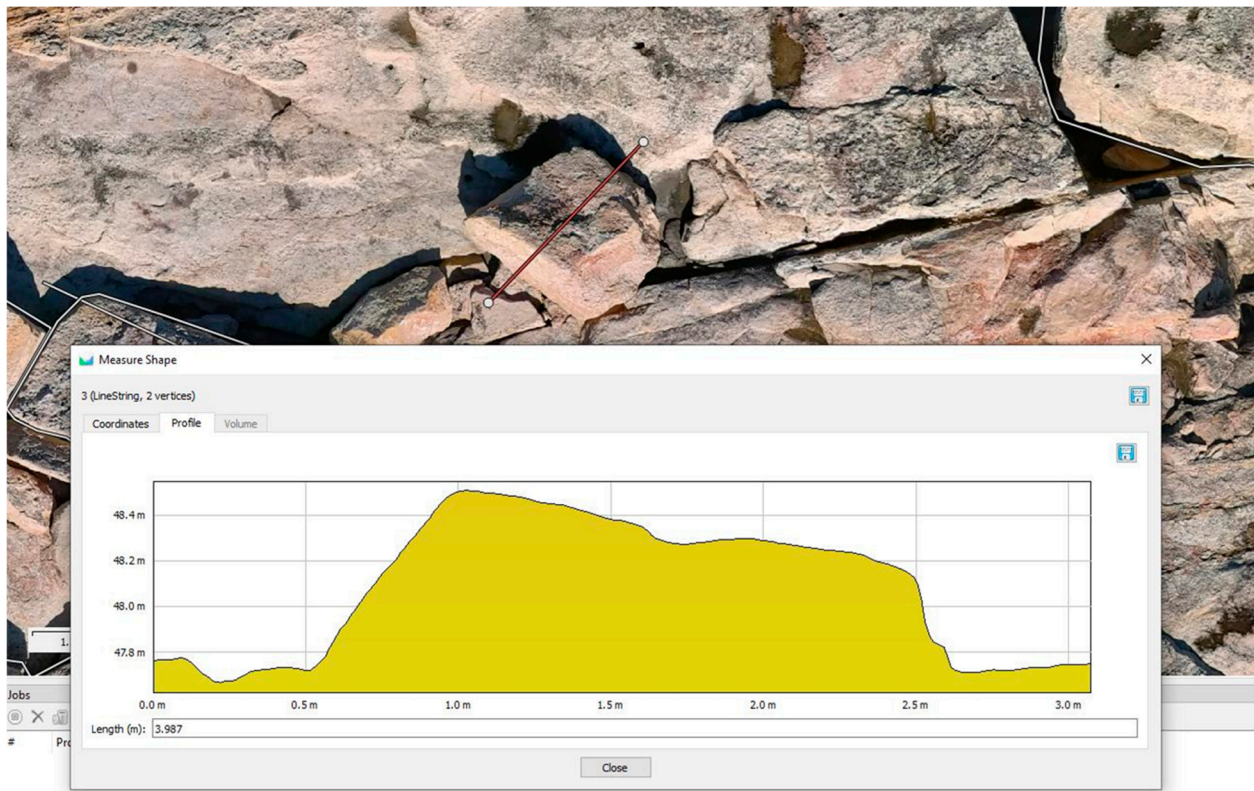
Figure 5. Polyline tool used to measure the C axis.

Figure 6. Polygon tool used to calculate the boulder surface area and volume using the Agisoft functionality.

3.4. Correlation Analysis

The correlation analysis was carried out between the axis measurements derived from the 3D model generated from the UAV images and those measured in-situ. This was carried out in order to assess the reliability of the data derived from the 3D model, when compared to that collected in-situ. Similarly, a correlation analysis was carried out between

the boulder volume as calculated from the in-situ collected A, B and C axis dimensions and the different methods applied to calculate volume from the 3D model. In all cases, a Spearman's rank correlation was used due to the type of data distribution.

3.5. Assessment of the Individual Boulder Volume from the Models Generated Using the SfM Techniques

As a further validation of the boulder volume results and to infer which of the tested methods is the most accurate, six boulders were identified, and their volume was measured from the individual models created using the SfM technique. Through this technique, a model is generated from a series of highly overlapping photographs (90%) taken around the object.

Between 70 and 100 photos were taken using a Moto G7 power 12 MP mobile camera with a f/2.0 lens. The images were taken from the ground around each boulder and from different angles and elevations, in order to cover the entire exposed surface area. Similar to the coastal 3D model, the models for each of the six boulders were generated on Agisoft Metashape Ver 1.8.0.

Upon uploading and aligning the photos, a dense point cloud and a polygonal mesh model were generated. Any missing parts of the boulder that could not be photographed, such as the bottom side, were closed using the 'close holes' tool in the mesh function. The model was scaled by inserting markers at either end of a ruler of known length that was placed on each boulder. These markers were subsequently used to generate a scale bar. The mesh model was used to measure each boulder's volume (Figure 7). This was then compared to the volumes obtained from the other calculation methods mentioned previously, in order to assess which method is the most accurate.

Figure 7. Workflow for the creation of individual boulder models on Agisoft Metashape for volume calculation.

4. Results

4.1. A, B and C Axis Dimensions

The frequency distribution of the A, B and C axis dimensions of the 198 boulders, as identified and measured in-situ and from the 3D model, are presented as histograms in Figure 8. In each measurement method (i.e., in-situ, model maximum and model average) they show a fairly similar distribution for all axis dimensions. For the A and B axes, the distribution is skewed towards the smaller measurements with the highest frequencies registered between 1.5 m and 2.5 m for the A axis and between 1 and 2 m for the B axis. This does not reflect the overall size distribution of the boulders at the site but is limited to the boulder sizes from the previous study that could be easily identified.

The data distribution for the three axes is shown in Figure 9. Although the axis dimensions distribution are very similar for the three methods, the highest similarity can be seen between the in-situ and the average model measurements. A slightly greater number of outliers was observed in both the average and maximum model measurements.
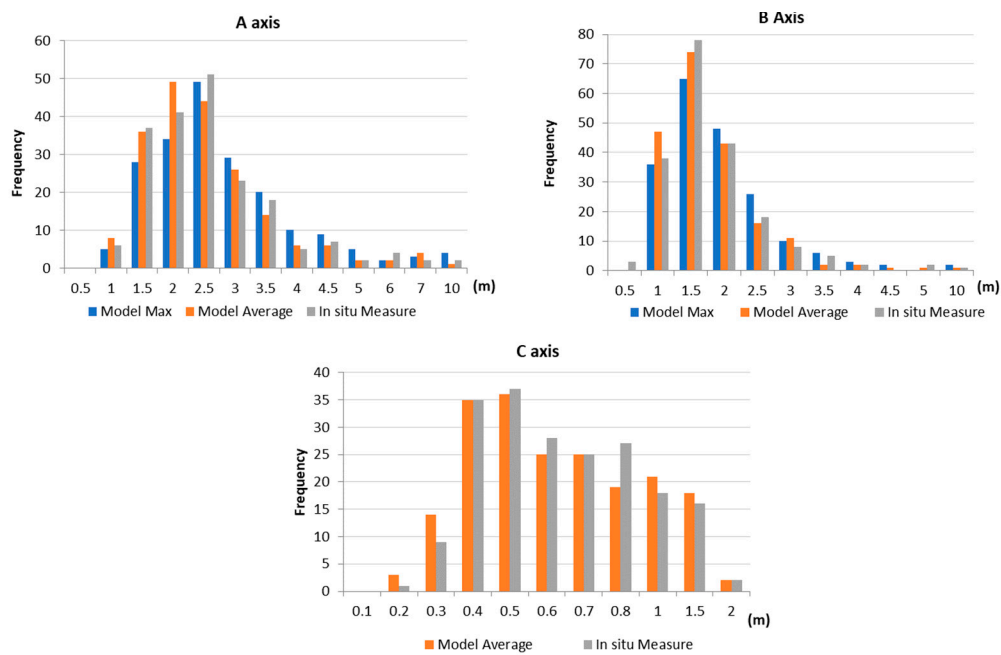
Figure 8. Histograms for the A, B and C axis maximum, average and in-situ measurements.
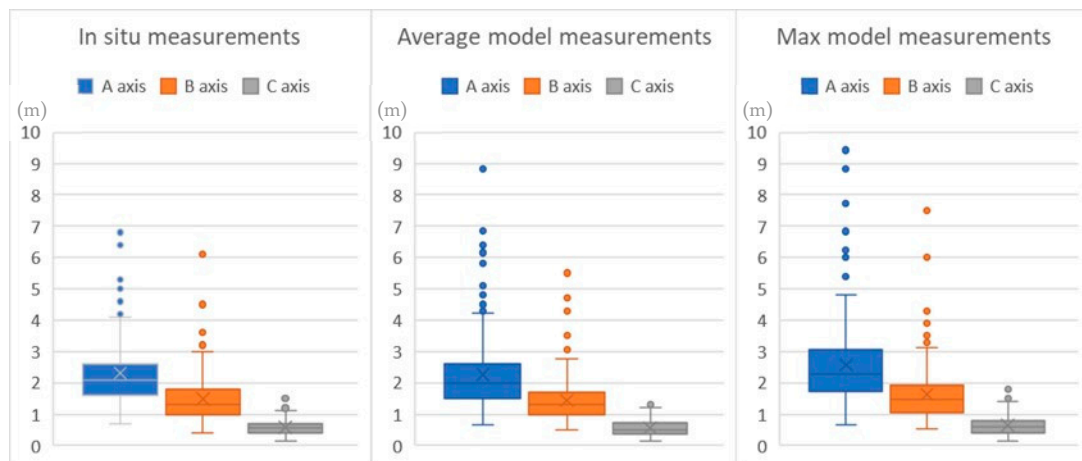

Figure 9. Box plots showing the data distribution for the A, B and C axis dimensions.

The correlation between the physical measurement and the model average measurement of the A and B axes at 0.95 and 0.91, respectively, is very strong and the *p*-value is less than 0.01 (Table 1). Similarly, the correlation between the in-situ measurements and the model maximum dimensions is also very strong (0.94 and 0.90), with a similar level of statistical significance.

Since the actual C axis could rarely be measured directly from the model, the data presented are only those for the model average and physical dimensions. As expected, the range of values is more limited for this axis and the distribution is less skewed as this dimension is generally controlled by the geology or bed thickness. The correlation between the two datasets is slightly lower and stands at 0.81, which is also significant. The *p* value, similar to the A and B axes, is less than 0.01, indicating that the correlations are statistically significant.

Table 1. Spearman's rank correlation statistics between the in-situ measurements and the model maximum and model average measurements for the A, B and C axis dimensions.

	Correlation between In Situ Measurements and Model Maximum Dimensions		Correlation between In Situ Measurements and Model Average Dimensions	
		p(uncorr)		*p(uncorr)*
A axis	0.94	<0.01	0.95	<0.01
B axis	0.90	<0.01	0.91	<0.01
C axis	0.77	<0.01	0.81	<0.01

Notwithstanding the high correlations, some differences were observed between the in-situ and model maximum and average dimensions for each axis, as can be seen in Figure 10. The in-situ measurements have been sorted in ascending order for ease of reference. The maximum model dimensions generally tend to be higher than the in-situ measurements, however some lower values were still observed. The average model dimensions tend to show both higher and lower values than the in-situ measurements.

The percentage difference between the in-situ dimensions and the modelled maximum/average axis dimensions was calculated for each boulder. The results are shown in the histograms in Figures 11–13, which respectively show the percentage differences between the following:

i.   the model maximum and model average dimensions for the A and B axes;
ii.   the model maximum dimensions and the in-situ measurements for the A and B axes;
iii.   the model average and in-situ measurements for the A, B and C axes.

Data in Figure 11 shows that for around half of the boulders, the difference between the maximum and average dimensions taken from the model, is less than 10%. The distribution in each category is relatively similar for both axes except for the 10% to 20% range, which is slightly higher for the A axis than for the B axis.

The differences between the model dimensions and the in-situ measurements were a range of positive and negative values, indicating that it is possible to overestimate and underestimate the measurements from the model, when compared to the dimensions taken physically in the field (Figure 10). For example, the A axis of boulder 3 was measured on site at 3.4 m, whilst the maximum and average dimensions derived from the model were 3.2 and 3.8 m, respectively. The in-situ measurements tend to show more occurrences of negative differences, when compared to the maximum dimensions derived from the model (Figure 12). This outcome is to be expected since the in-situ measurements represent more conservative average boulder dimensions. Conversely, when comparing, the model average to the in-situ measurements, the latter are generally higher than the former, indicating a tendency to estimate lower average values from the model, as seen in Figure 13. For the majority of boulders, the percentage difference for the A and B axes is less than 20%.
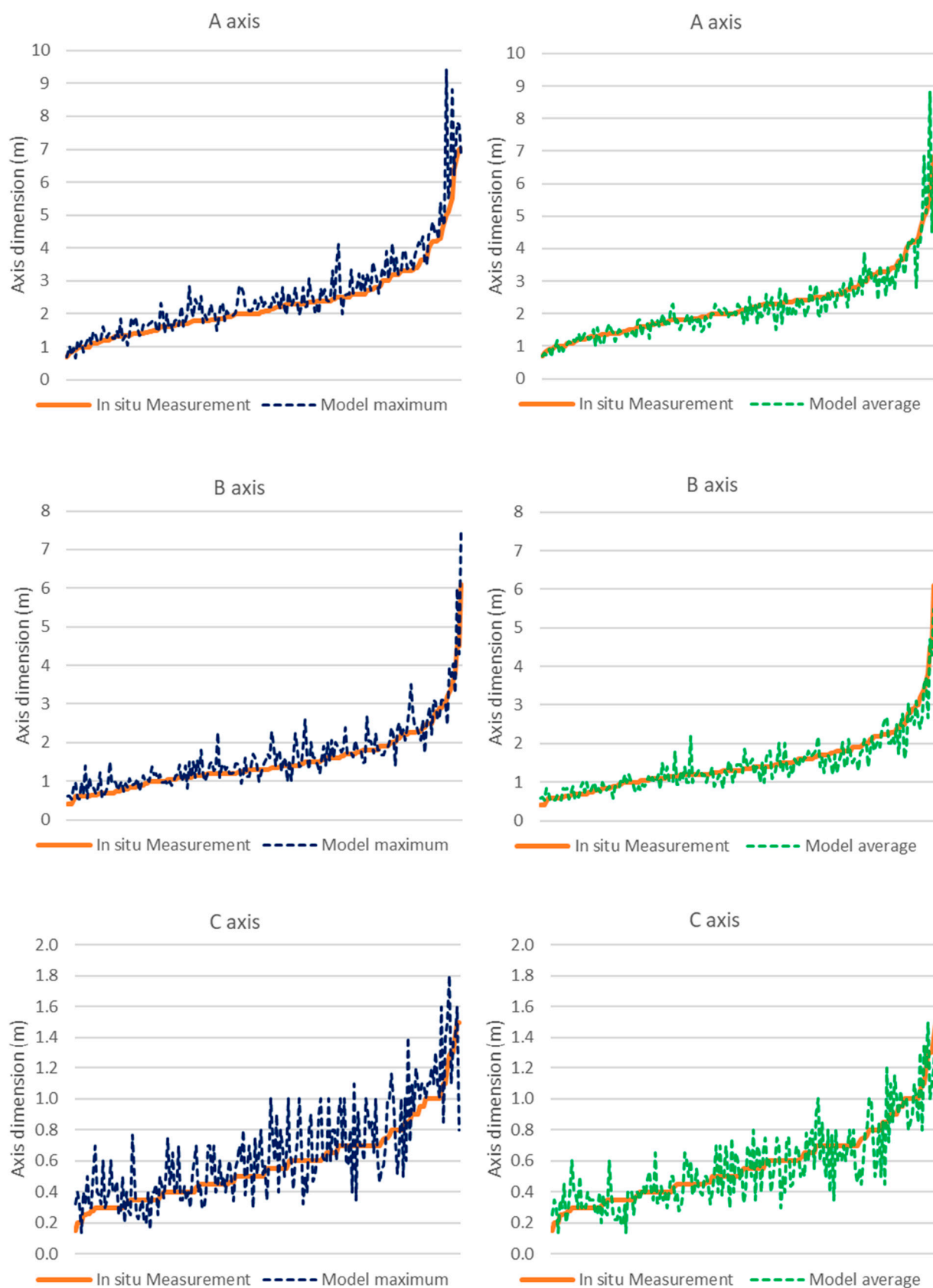
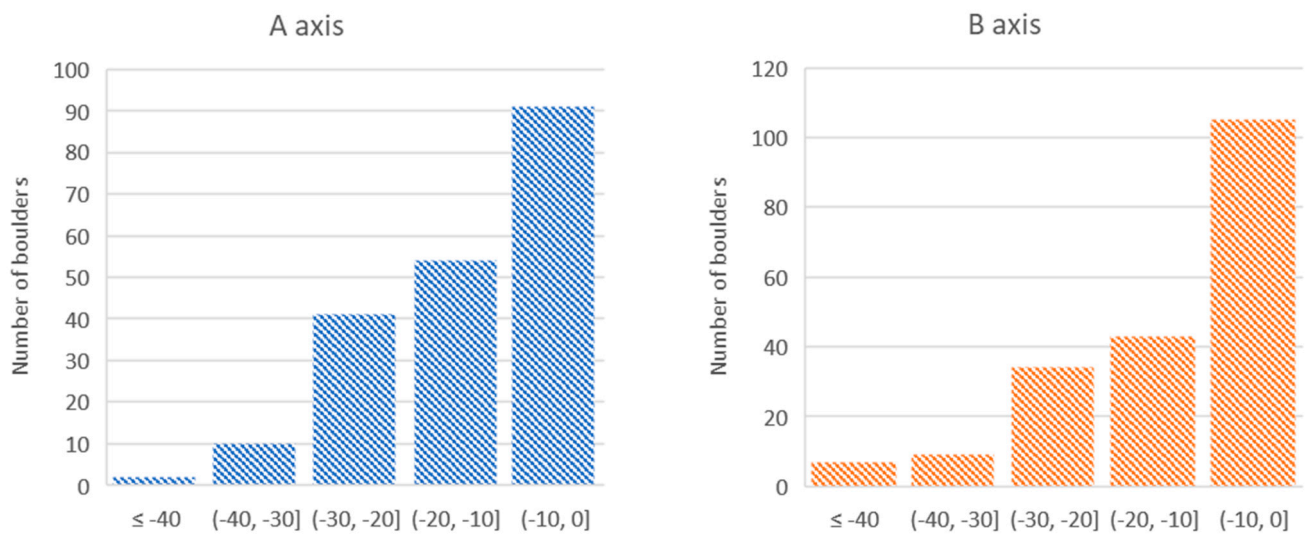**Figure 10.** Differences between the in-situ axes measurements and those derived from the model.

Figure 11. Percentage difference between the model maximum and the model average dimensions for the A and B axes.
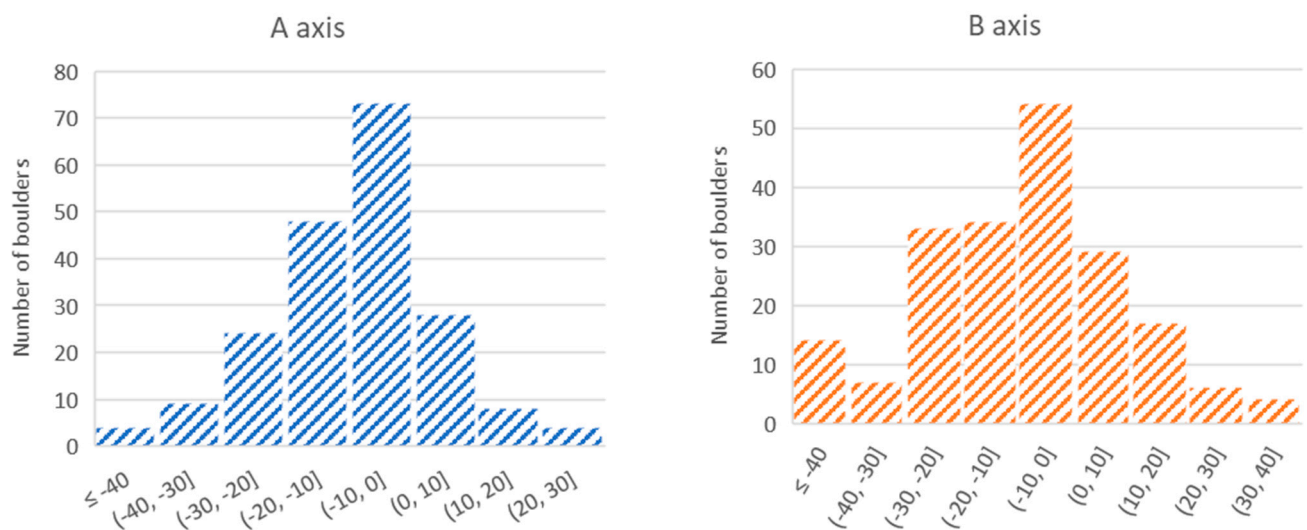

Figure 12. Percentage difference between the model maximum and the in-situ measurements for the A and B axes.

For the C axis, the difference between the average and in-situ measurements is more equally spread across both the positive and negative categories. This is probably due to the difficulty in obtaining this dimension from the model by direct measurement, as in most cases it was derived. The frequency of greater differences (>20%) increased considerably for this axis (Figure 13).

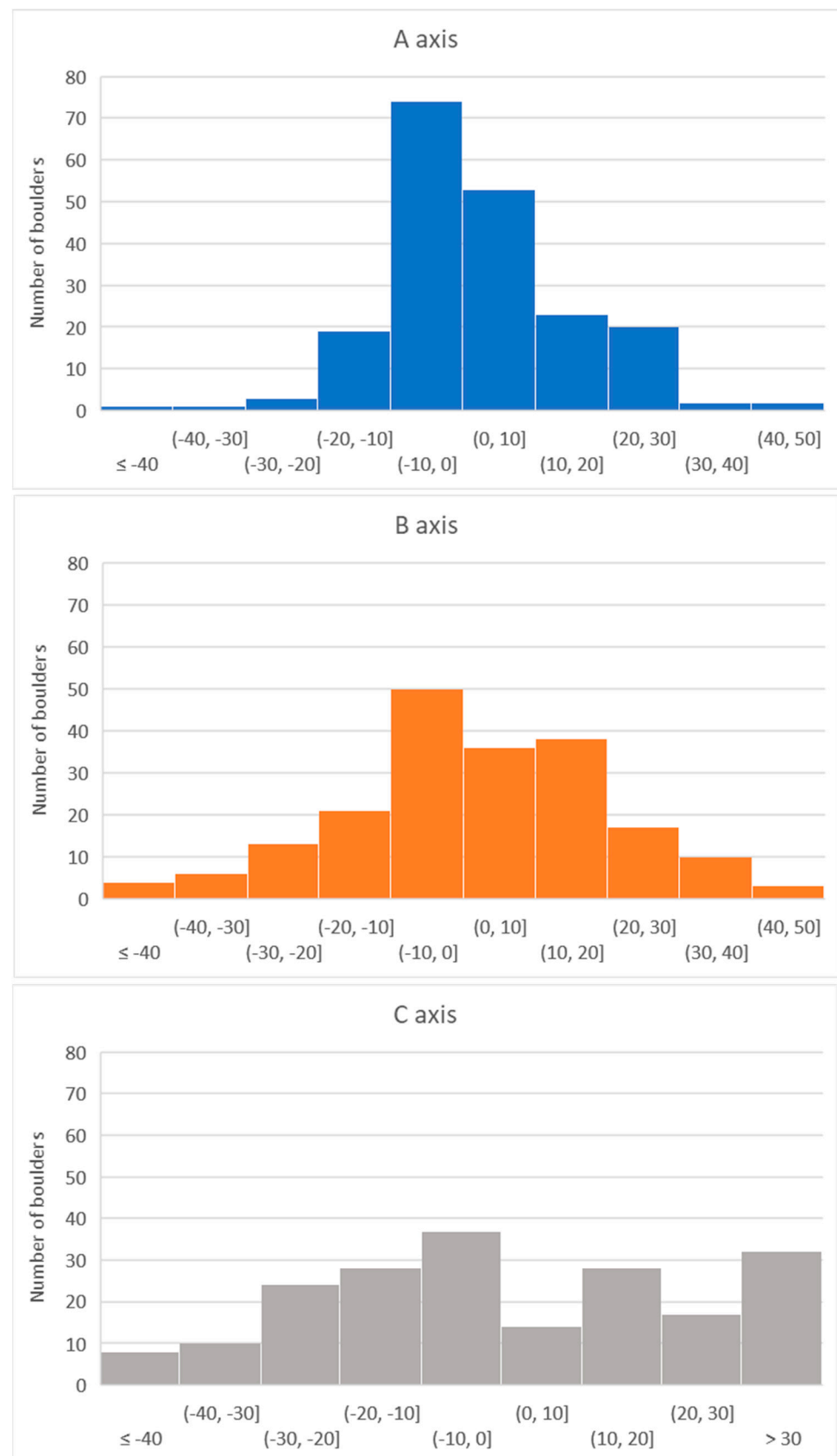**Figure 13.** Percentage difference between the model average and the in-situ measurements.

4.2. Boulder Volume Measurements

The boulder volume was calculated using various methods and their results were compared. These methods include geometric formulas using the axis dimensions described above, the multiplication of the surface area derived from the model by the average height, and by using the volume calculation functionality provided by the software itself, using the best fit option or custom plane option. The distribution of the boulder volume for each method is shown in Figure 14.
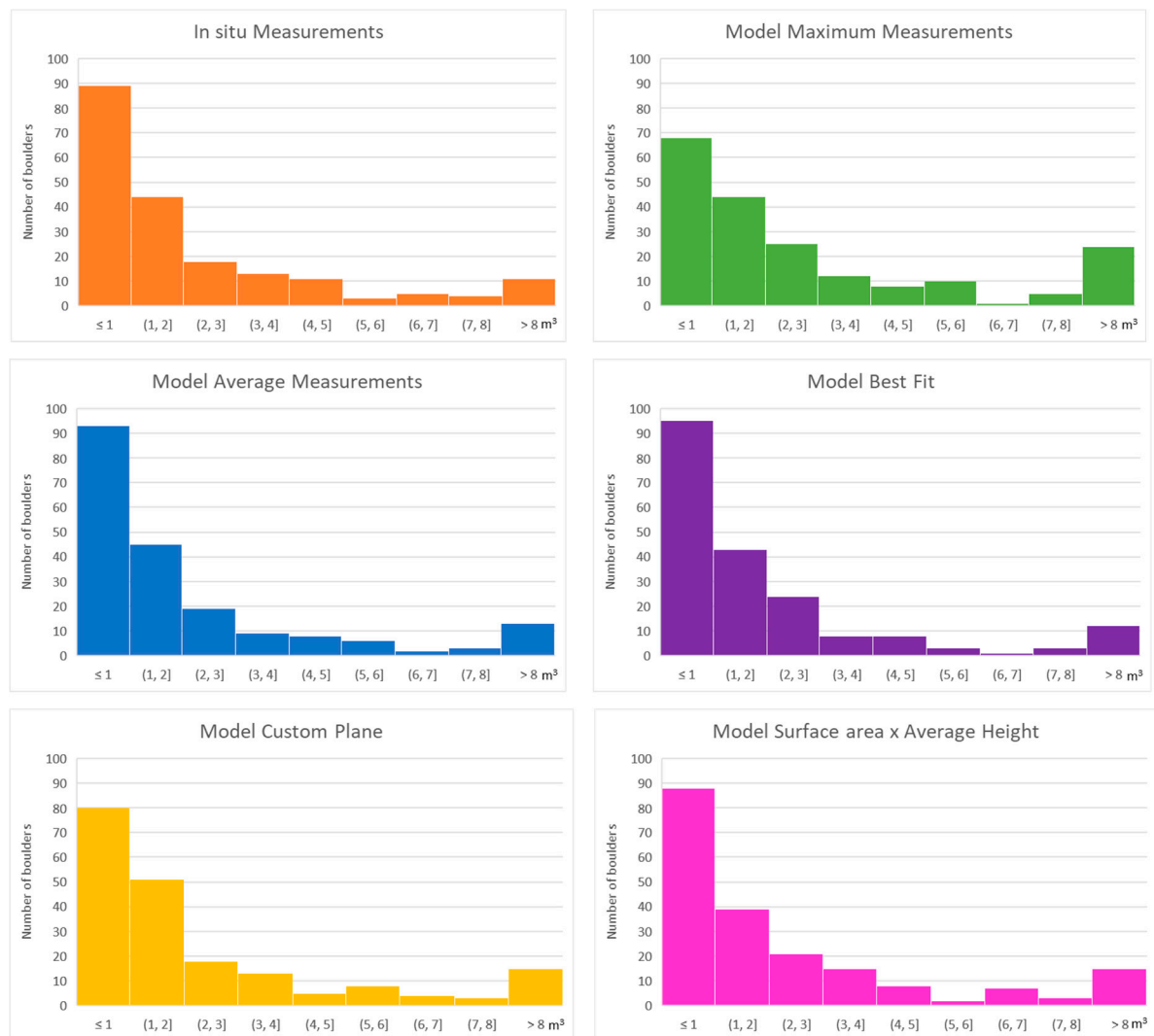

Figure 14. Histograms showing the distribution of the boulder volume, according to each method of calculation.

The highest frequencies are observed in the categories below 2 m^3, indicating that the data is skewed towards the smaller boulders. Although some of the volume calculation methods show similar results, some differences are observed. The largest variance between methods seems to occur in the lowest volume categories (0.5 m^3 and 1 m^3). For example, in the 0.5 m^3 category, there is a striking difference between the maximum model measurement and the best fit method whilst the results for the other methods are fairly similar. In the 1 m^3 category, similar results were obtained for the in-situ measurements: on one hand, the average model measurements and the surface area × height, and on the other, the maximum model measurement, the best fit and the custom plane methods.

The most similar distribution across all categories seems to be between the in-situ, the average model measurements and the surface area multiplied by the height methods. The

maximum model measurements, as expected, produce larger boulder volumes whilst the best fit method tends to produce smaller values.

The above observations are confirmed by the correlation tests carried out between the physical measurement and the modelled methods. Although a very strong positive correlation was obtained for all methods, as can be seen in Table 2 (r value varying between 0.96 and 0.91), the highest correlation was observed for the model average and the in-situ measurement methods.

Table 2. Correlation coefficient between the boulder volume calculated using the in-situ dimensions and the different methods derived from the model.

	In-Situ Measurements	*p* Value
Model average measurements	0.96	<0.01
Model maximum measurements	0.94	<0.01
Best fit	0.91	<0.01
Custom plane	0.92	<0.01
Surface area × average height	0.93	<0.01

Notwithstanding these positive correlations, the analysis at specific boulder levels shows a variance between the results, as calculated by the different methods. The variance for each method, compared to the physically measured boulder volume is shown in Figure 15. The difference can be either positive or negative. For ease of reference, the data for the physical boulder volume has been sorted in ascending order.

The figures show that, when compared to the volume derived from the in-situ measurements, the model maximum dimensions generally tend to overestimate the volume, whilst using the best fit option underestimation is more likely. To a lesser extent, the model average measurements also produce slightly lower volumes than the in-situ measurements. With the other methods, the differences are approximately equally spread between positive and negative differences.

The histograms showing the frequency of the percentage difference for each method and the box plots in Figure 16 also reflect this trend. For all methods, except for the maximum model dimensions method, between 1/3 and 1/2 of the samples registered a difference of ± 20%, whilst another 1/4 to 1/3 registered a difference of between ±20% and ±40%.

Another way of assessing these differences is to compare the total volume of all of the boulders, as calculated by the different methods. These results are presented in Table 3.
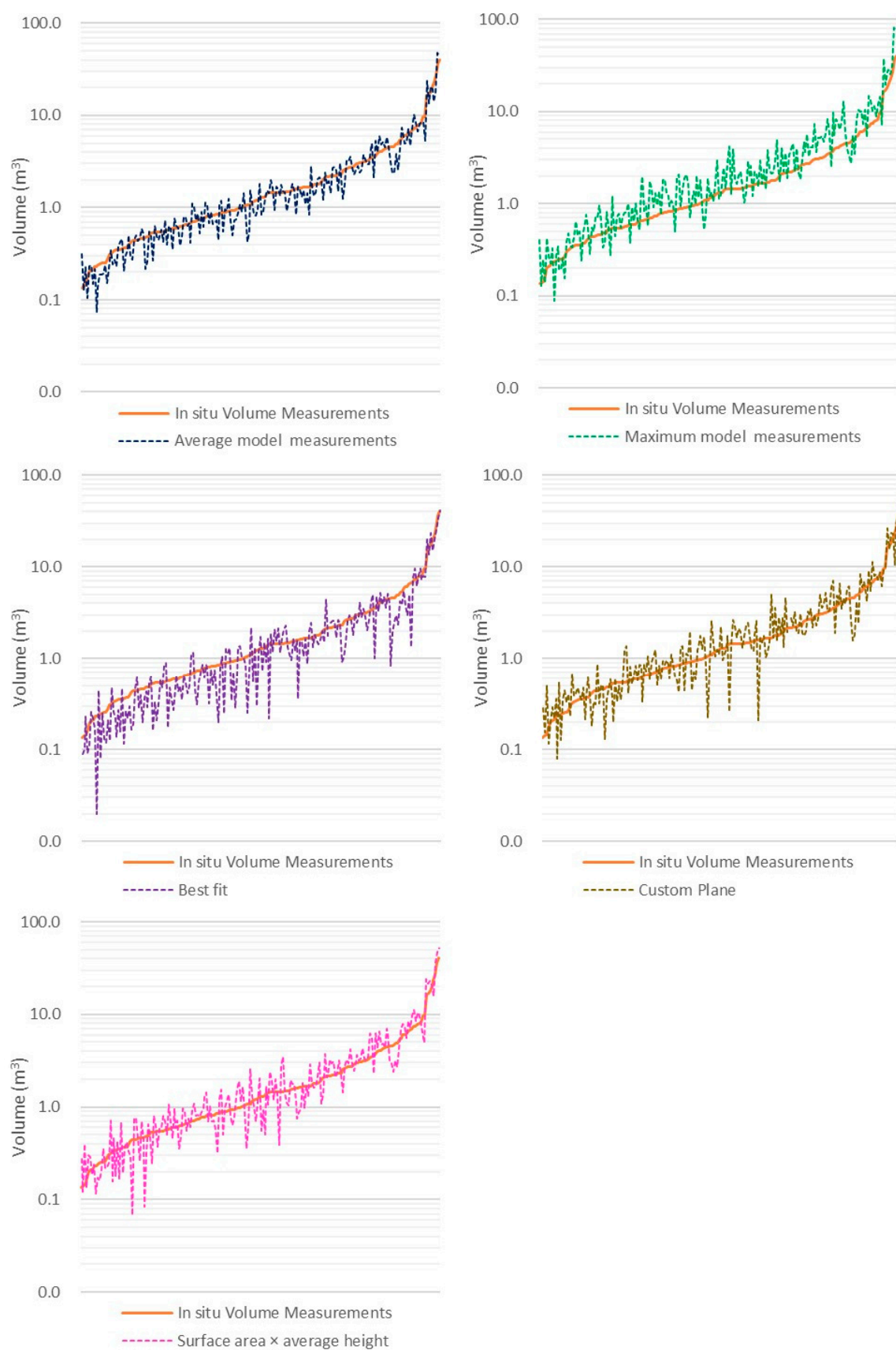
Figure 15. Volume calculated from the in-situ measurements for each boulder, compared to the volume calculated by each of the other methods from the model.
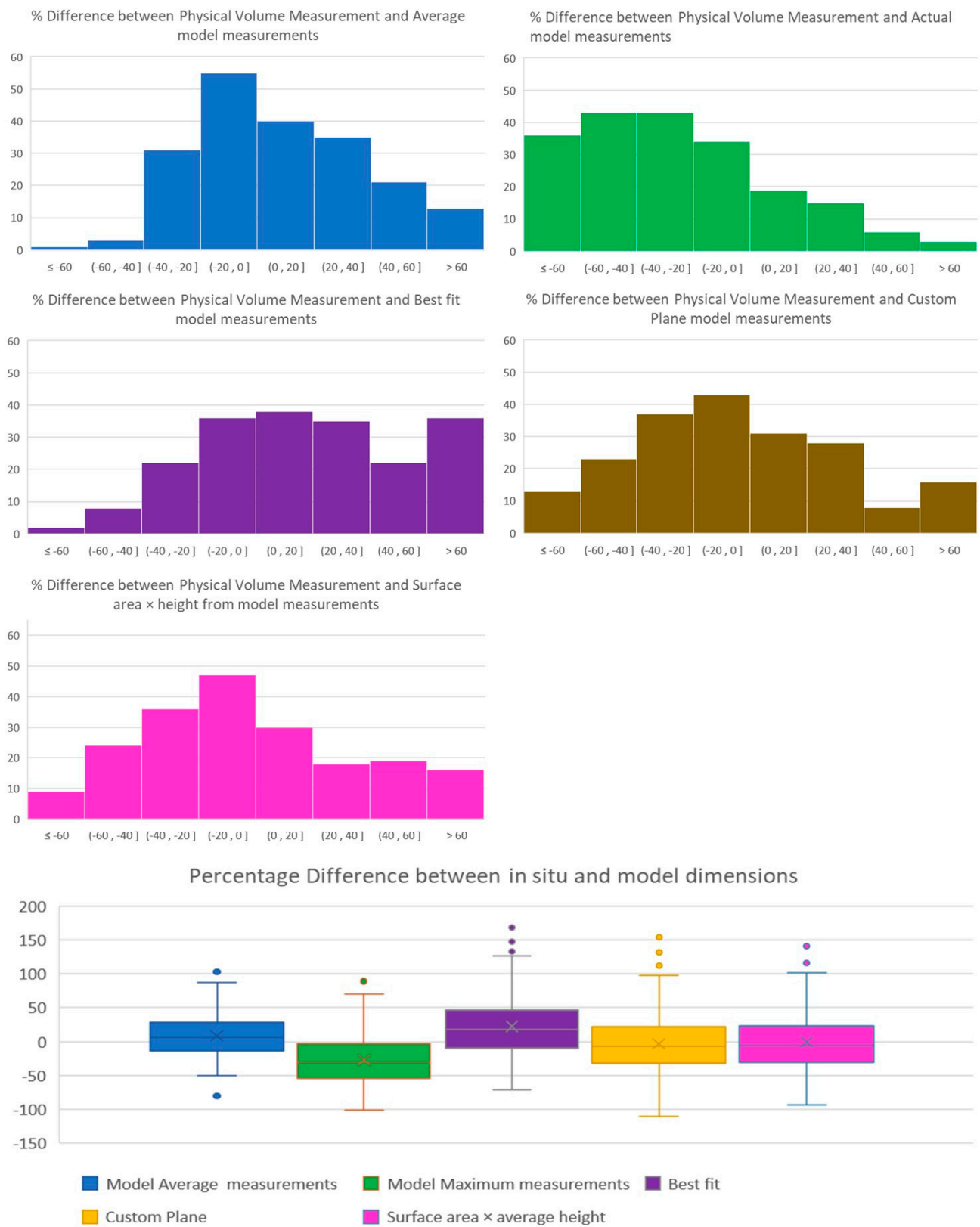
Figure 16. **Top**: Histograms showing the frequency of the percentage difference between the model volume calculation and the physically measured volume. **Bottom**: Box plots showing the data distribution.

Table 3. Sum of the volume of all boulders measured, for each method.

Method	In-Situ Measurements	Average Model	Maximum Model	Best Fit	Custom Plane	Surface Area × Height
Total volume (m^3)	554.54	541.24	840.85	502.49	600.96	626.24
Difference from the physical measurements (m^3)		−13.30	286.32	−52.05	46.42	71.70
Percentage difference from the physical measurements		−2.43%	41.04%	−9.85%	8.03%	12.15%

4.3. Boulder Volume Measurement using SfM

Given that boulders are rarely perfectly cuboid in shape, some over or under estimation of their volume is to be expected when calculating using geometric formulas. In order to arrive at the most accurate volume estimation possible, the volume for six individual boulders was measured using the SfM technique. The criteria for choosing these specific boulders were related to the irregularity of the boulder shape, size and position, to assess how these factors could have influenced the volume calculations described above. The chosen boulders and their particular characteristics are listed below, and the boulder images can be seen in Figures 17–22. The yellow scale rule used for scale is 50 cm long. Their respective location is shown in Figure 23.

i. Boulder 1 is of a roughly triangular shape with an irregular thickness, positioned on rough, slightly sloping ground;

ii. Boulder 2 is also irregularly shaped; its surface has been partially hewn out as it formed part of a saltpan. During transportation it was overturned and now lies on its side (C axis);

iii. Boulder 3 is roughly cuboid and lies partially inclined on a low scarp;

iv. Boulder 4 is steeply imbricated and lodged between other boulders at the top of a boulder ridge. Its shape is also roughly cuboid;

v. Boulder 5 is irregularly shaped and is located at the front of a cluster of boulders at the foot of the ridge;

vi. Boulder 6 is a very large irregularly shaped mega-boulder of varying thickness. The A and B axes were measured at 7.8 and 7.5 m, respectively. It mostly overlies the shore platform but partially lies over a cluster of boulders that have accumulated in a low channel within the platform itself.

Figure 17. Boulder 1—Triangular boulder of an irregular thickness on rough sloping ground.

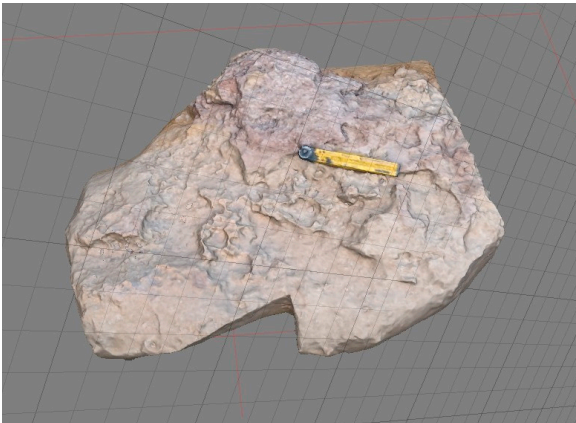**Figure 18.** Boulder 2—Irregularly shaped boulder on a flat surface.

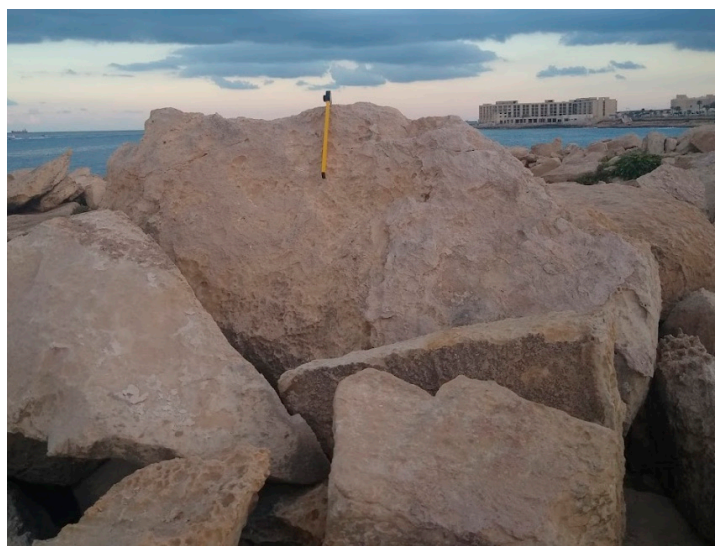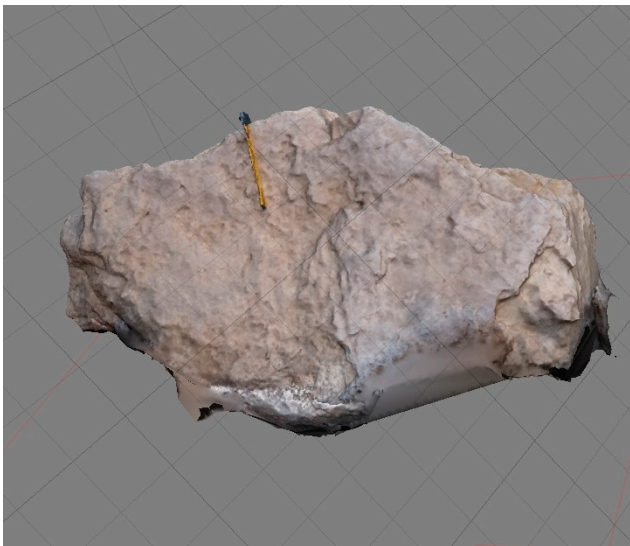**Figure 19.** Boulder 3—inclined on a scarp.

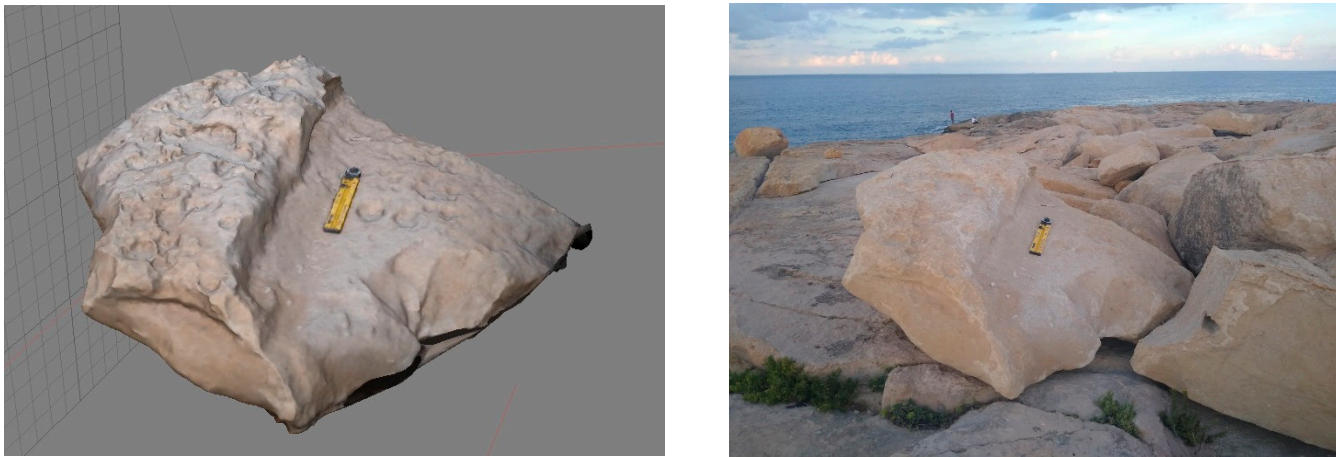**Figure 20.** Boulder 4—imbricated on a ridge.

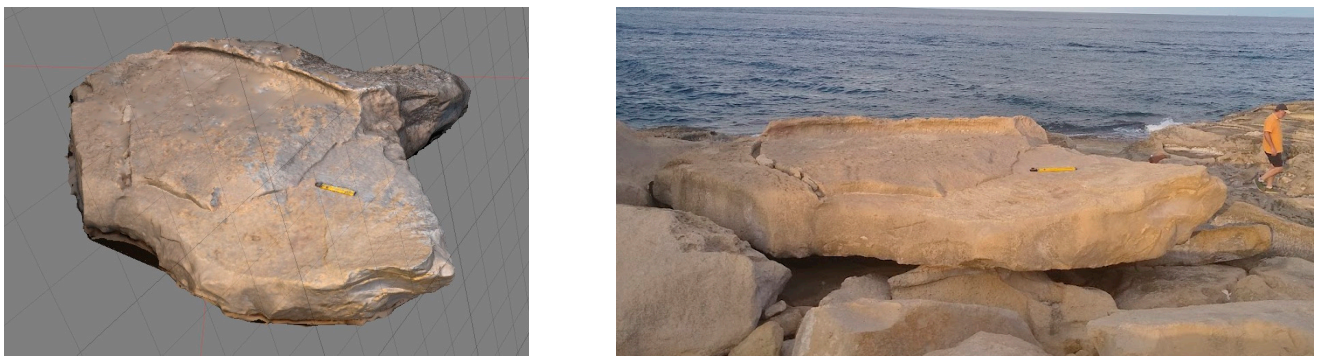**Figure 21.** Boulder 5—at the front of the cluster/ridge.

Figure 22. Boulder 6—Very large irregularly shaped boulder.

Figure 23. Location of selected boulders, the volume of which was calculated using SfM techniques.

The volume results for the six individual boulders measured using SfM and the corresponding volumes obtained by the other methods described above, can be seen in Table 4, whilst the differences between the SfM derived values and those obtained from the other methods can be seen in Table 5.

Table 4. Boulder volume measurements including the SfM data for six individual boulders. Boulder number in bracket (first column) refers to the original ID attribute from the whole dataset of site boulders.

Boulder (No.)	Volume Calculation Methods						
	In-Situ Measurements	Average Model	Maximum Model	Best Fit	Custom Plane	Surface Area × Height	SfM
	(m³)	(m³)	(m³)	(m³)	(m³)	(m³)	(m³)
1 (65) irregular shape	1.29	1.79	2.93	1.74	2.23	2.02	**1.46**
2 (20) irregular shape	1.44	1.58	1.84	2.11	2.14	1.35	**1.71**
3 (424) inclined on a scarp	2.7	3.15	3.60	2.95	2.97	2.93	**2.53**
4 (252) imbricated on a ridge	1.60	0.85	1.21	1.56	2.58	1.17	**1.54**
5 (225) in front of a cluster	3.02	2.86	7.34	2.91	2.78	3.64	**2.91**
6 (439) very large	36.52	47.52	81.90	34.36	35.7	47.52	**27.05**

Table 5. Percentage differences between the SfM derived volume and the volume derived from other methods. Shading represents the degree of difference: green <20%, yellow 20% < 40%, red >40%.

Boulder (No.)	% Difference from the SfM Volume					
	In-Situ Measurements	Average Model	Maximum Model	Best Fit	Custom Plane	Surface Area × Height
	%	%	%	%	%	%
1 (65) irregular shape	−11.64	22.60	100.68	19.18	52.74	38.36
2 (20) irregular shape	−15.79	−7.60	7.60	23.39	25.15	−21.05
3 (424) inclined on a scarp	6.72	24.51	42.29	16.60	17.39	15.81
4 (252) imbricated on a ridge	3.90	−44.81	−21.43	1.30	67.53	−24.03
5 (225) in front of a cluster	3.78	−1.72	152.23	0.00	−4.47	25.09
6 (439) very large	35.01	75.67	202.77	27.02	31.98	75.67

The results show that the volume estimates closest to the SfM calculations were obtained from the physical measurements and the best fit option. As often remarked in the literature [31], the absolute model dimensions may produce highly overestimated volumes and this was the case for four of the tested boulders in this study (boulders 3, 4, 5 and 6). For the other two boulders, the more accurate volume estimation can be attributed to a lower axis value, as the boulders were not fully visible on the model due to their particular position or location (inclined on ridge).

The greatest differences across all methods were found in the largest boulder (no. 6), which is actually a block, since its B axis exceeds 4.2 m. In this case, all volume calculations were overestimated, when compared to those by SfM. The clast has an irregular shape and thickness and is not resting on level ground. This highlights the difficulty of assessing and accurately measuring such large clasts, both physically and through the model. The most accurate methods were the best fit with a difference of 27%, the custom plane (32%) and the physical measurements (35%). The average model and surface area × height results were some 75% higher, due to an overestimation of the C axis value.

5. Discussion

5.1. Boulder Dimension Measurements

The principal aim of this study was to assess the reliability of remotely acquired data, when compared with data obtained directly from the field. The customary way to measure clasts is to measure their A, B and C axis dimensions; however, when calculating the volume using this data, it is likely for the result to be overestimated, as boulders are rarely perfectly cuboid in shape. In order to avoid this overestimation, the axis dimensions

obtained from the field were more conservative, reflecting average axis values, whilst in this study, both the maximum and average axis dimensions were extracted from the model. This averaging technique is reflected in the differences observed, when comparing the data collected in the field to the maximum axis dimensions and the volume derived from the 3D model. The C axis maximum values were not compared as in most cases this was not possible to measure directly.

For the majority of comparisons between the A, B and C axis dimensions, the differences did not exceed ± 20%. The lowest difference was found between the average and in-situ measurements for the A axis, where around 2/3 of the samples show a difference of ±0 to 10%, whilst for the B axis, and to a greater extent the C axis, the differences are more equally staggered across the categories. This could be due to the arbitrary and subjective way in which the average dimensions are measured which may differ, depending on the size, view and accessibility of the boulder being measured.

Notwithstanding these differences, the results show that there is a strong correlation between the axis dimensions measured physically on site and both the average and maximum model dimensions. As expected, the strongest correlation was observed with the model average measurements. The A and B axes showed the highest correlations (0.94 and 0.91). These were the most straightforward to measure from the model. In some respect, it was easier to calculate the average measurements from the model rather than on site, especially when the boulders were large and/or high and could not be assessed in their entirety at ground level. In such cases, obtaining an overhead view from a model greatly enhances the assessment to determine the degree of irregularity of the boulder shape and the best average dimensions to measure. Effectively, the largest percentage differences were observed in some of the largest boulders with A and /or B axes that exceeded 2 m.

The C axis values showed a slightly lower correlation at 0.81. This may be attributed to the fact that in the majority of cases, this axis could not be measured directly and had to be calculated from the difference between the boulder and the ground at various locations. When boulders have an irregular thickness or are positioned inclined against a scarp or other boulders, it is easier to miscalculate this value. More than half of the boulders found in an inclined or imbricated position showed a 15% or more difference in this axis dimension.

The boulder volume was calculated using geometric formulas and the axis dimensions obtained on site and from the model using the software volume calculation functionality. The correlation statistics were all very strong, exceeding 0.9 with a high statistical significance (<0.01). The highest correlation at 0.9604 was also found between the in-situ and model average dimensions.

At boulder level, a notable difference in the volume calculation was observed in specific circumstances, which are mainly related to the boulder position/imbrication and/or ground surface irregularity, due to the presence of slopes, scarps or other underlying boulders. Such circumstances lead to an under- or overestimation of the C axis, due to the difficulty of measuring precisely from the model. Some differences were also observed in the A and B axes in some of the imbricated boulders and in the very large boulders or blocks.

It was observed that with the best fit function, an overestimation of the volume is a possibility when the ground is uneven, due for example, to the presence of scarps. When tabular boulders rest inclined against scarps or imbricated on other boulders, the space between the base of the boulder and the scarp may be included with the boulder volume.

The highest variance between the in-situ and the best fit model volume estimations occurred when the boulders were located within or on top of a cluster and their C axis could not be clearly evaluated. The model-derived volume was generally lower when the boulder surface was level with other surrounding clasts, and higher when the boulders were found overlying other clasts or very rough terrain. In such cases, the custom plane values were found to be closer to the physical measurement values.

One issue with the volume calculation using the system functionality is the requirement to draw a polygon around the boulder to be measured. The preciseness of this

polygon, which might be impacted by issues, such as shadows or partial visibility, bears upon the accuracy of the volume. An automated way of identifying the boulder perimeter, such as through an analysis of the surface roughness, would certainly mitigate errors due to the inaccuracy of these polygons.

As often mentioned in the literature, the maximum dimensions tend to overestimate the boulder volume e.g., [32], and this is also reflected in these results. All of the histograms in Figure 14 show a similar volume distribution, except for that representing the volume derived from the maximum model dimensions, which is skewed towards the higher values. When comparing the total volume of all boulders tested (Table 3), maximum axis dimensions from the model produced the highest volume overestimation of approximately 41%, when compared to the in-situ measurements. The closest was the volume obtained from the model average dimensions, with a difference of −2.4%. The results from the other three methods varied from −9.85% to 12.15%. The accuracy of the boulder volume is significant when used in numerical models to estimate, for example, the wave flow velocity or inundation for a coastal hazard assessment. Overestimation is likely when numerical models are applied to non-cubic boulders [8]. Further assessment on how these different volume calculation methods impact the numerical model results. is a possible avenue for future research.

For a more accurate boulder volume estimation, the models created from techniques, such as terrestrial laser scanners [31,33,34], photogrammetry and SfM [9,35–38], and point clouds generated from the UAV images [17] have been used. In this study we have used photogrammetry and SfM to create models of six individual boulders, and compared the volume derived to that estimated from the other methods described above. The most similar is that obtained through physical observations and direct field measurements, at least for the boulder sized clasts. The precise volume estimation for the larger block was found to be elusive, possibly due to shape irregularity. The best fit option also produced results comparable to the SfM models, whilst the results from the model average volume varied from minimal to significant differences. These results seem to indicate that whilst the model average dimensions may provide an adequate volume estimation (such as when boulders are very large (blocks) or when they are partially visible due to the position of adjacent boulders) the best fit option may be more reliable.

This study has been carried out in an area where the size and shape of the boulders is, to a certain extent, determined by the geology (sedimentary limestone beds) and by the structure (conjugate joint sets and bedding planes). A similar analysis of other boulder sites in different geological settings, (e.g., with more rounded boulders) may provide further insights on the application of boulder measurement techniques and their comparisons.

Although large volumes of data may be more efficiently collected remotely, certain geomorphological constraints may still necessitate some degree of ground truthing for an enhanced accuracy. Other boulder attributes, such as lithology and density, cannot be assessed or sampled remotely [9], requiring a physical presence on site. Site fieldwork also provides the opportunity to observe and identify features at smaller scales that may otherwise be missed, such as abrasion marks, detachment scars and tight discontinuities. Immersion in the field and taking the time to look out for and observe the general surroundings, as well as the finer details, provides a more holistic experience of the site and possibly a better understanding of the operative processes [39]. It is a unique experience which is hard to replicate on a screen.

5.2. Biases and Limitations

Being familiar with the location and having boulder photos at hand, has enabled the assessment of the C axis dimension to be carried out with knowledge of the site and any boulder imbrication. In the case of inaccessible or unfamiliar sites, this would not be possible. Having said that, it was still hard to identify most of the smaller boulders that were physically measured in the original study, either simply because they were not easy to identify from the photos or because they had been transported to a new location by

waves. Thus, the data analysed in this study tends to be biased in favour of larger clasts that generally exceed 1 m in the A axis and 0.5 m in the B axis dimension.

Another issue that could have skewed the results is that of personal subjectivity when deciding on average values, especially for the larger clasts. Sometimes, it is easier to assess the general shape of a boulder when viewing it from an overhead perspective, as from the 3D model, rather than moving around it on the ground. Thus, some discrepancies between the model and the physical dimensions may be attributed to this.

6. Conclusions

The aim of this study was to assess the reliability of remotely acquired data, by comparing coastal boulder dimensions and volume acquired from a 3D model generated from aerial images using an UAV, to the same data collected physically during fieldwork on site. The dataset covers 198 boulders.

The results indicate that there is a strong correlation between the boulder data collected on site (A, B and C axis dimensions and derived volume) and the data obtained from the 3D models generated from the aerial images acquired by UAV. For the majority of boulders, the percentage difference between the model average and the in-situ measurements are up to ±10% for the A axis and ±20% for the B axis. The variance for the C axis shows a more equally staggered distribution of percentage differences. This was to be expected, due to the difficulty of measuring this dimension directly from the model.

The analysis of the differences in boulder volume, as calculated by the different methods, shows that some methods, such as the average measurements derived from the models and the best fit options are perhaps more reliable than others to produce more accurate datasets.

The volume data were further validated using SfM techniques to calculate the boulder volume of six individual boulders. The results show that for the majority of the smaller sized boulders, the closest values to the SfM volume were derived from the physical measurements and the best fit functionality option. In the case of a very large boulder, all methods produced overestimations, when compared to the SfM derived volume.

It is not possible to determine boulder attributes, such as lithological composition and density, remotely, and certain geomorphological assessments, due to the boulder settings require physical onsite observations. However, this study has shown that the data acquired from the aerial images is a very effective tool for coastal monitoring, in terms of achieving a balance between the ease of access, time constraints, large volume and reliability of the data. The data shows that some methods, such as the average measurements derived from the models and the best fit options, are perhaps more reliable than others to produce more accurate datasets.

References

1. Paris, R.; Naylor, L.A.; Stephenson, W.J. Boulders as a signature of storms on rock coasts. *Mar. Geol.* **2011**, *283*, 1–11. [CrossRef]
2. Paris, R.; Fournier, J.; Poizot, E.; Etienne, S.; Morin, J.; Lavigne, F.; Wassmer, P. Boulder and fine sediment transport and deposition by the 2004 tsunami in Lhok Nga (western Banda Aceh, Sumatra, Indonesia): A coupled offshore–onshore model. *Mar. Geol.* **2010**, *268*, 43–54. [CrossRef]
3. Goto, K.; Miyagi, K.; Kawamata, H.; Imamura, F. Discrimination of boulders deposited by tsunamis and storm waves at Ishigaki Island, Japan. *Mar. Geol.* **2010**, *269*, 34–45. [CrossRef]
4. Terry, J.P.; Karoro, R.; Gienko, G.A.; Wieczorek, M.; Lau, A.Y.A. Giant palaeotsunami in Kiribati: Converging evidence from geology and oral history. *Isl. Arc* **2021**, *30*, e12417. [CrossRef]
5. Nott, J. Waves, coastal boulder deposits and the importance of the pre-transport setting. *Earth Planet. Sci. Lett.* **2003**, *210*, 269–276. [CrossRef]
6. Pignatelli, C.; Sanso, P.; Mastronuzzi, G. Evaluation of tsunami flooding using geomorphologic evidence. *Mar. Geol.* **2009**, *260*, 6–18. [CrossRef]
7. Nandasena, N.A.K.; Paris, R.; Tanaka, N. Reassessment of hydrodynamic equations: Minimum flow velocity to initiate boulder transport by high energy events (storms, tsunamis). *Mar. Geol.* **2011**, *281*, 70–84. [CrossRef]
8. Nandasena, N.A.K.; Scicchitano, G.; Scardino, G.; Milella, M.; Piscitelli, A.; Mastronuzzi, G. Boulder displacements along rocky coasts: A new deterministic and theoretical approach to improve incipient motion formulas. *Geomorphology* **2022**, *407*, 108217. [CrossRef]
9. Boesl, F.; Engel, M.; Rodrigo, C.E.; Galang, J.A.; Gonzalo, L.A.; Llanes, F.; Quix, E.; Brückner, H. Digital mapping of coastal boulders—High-resolution data acquisition to infer past and recent transport dynamics. *Sedimentology* **2020**, *67*, 1393–1410. [CrossRef]
10. Ruban, D.A. Finding Coastal Megaclast Deposits: A Virtual Perspective. *J. Mar. Sci. Eng.* **2020**, *8*, 164. [CrossRef]
11. Delle Rose, M.; Martano, P.; Orlanducci, L. Coastal Boulder Dynamics Inferred from Multi-Temporal Satellite Imagery, Geological and Meteorological Investigations in Southern Apulia, Italy. *Water* **2021**, *13*, 2426. [CrossRef]
12. Devoto, S.; Hastewell, L.J.; Prampolini, M.; Furlani, S. Dataset of gravity-induced landforms and sinkholes of the Northeast Coast of Malta (Central Mediterranean Sea). *Data* **2021**, *6*, 81. [CrossRef]
13. Devoto, S.; Macovaz, V.; Mantovani, M.; Soldati, M.; Furlani, S. Advantages of Using UAV Digital Photogrammetry in the Study of Slow-Moving Coastal Landslides. *Remote Sens.* **2020**, *12*, 3566. [CrossRef]
14. Gomez-Pazo, A.; Perez-Alberti, A.; Trenheile, A. Recording inter-annual changes on a boulder beach in Galicia, NW Spain using an unmanned aerial vehicle. *Earth Surf. Processes Landf.* **2019**, *44*, 1004–1014. [CrossRef]
15. Perez-Alberti, A.; Trenhaile, A. An initial evaluation of drone-based monitoring of boulder beaches in Galicia, north-western Spain. *Earth Surf. Processes Landf.* **2015**, *40*, 105–111. [CrossRef]
16. Sedrati, M.; Morales, J.A.; El M'rini, A.; Anthony, E.J.; Bulot, G.; Le Gall, R.; Tadibaght, A. Using UAV and Structure-From-Motion Photogrammetry for the Detection of Boulder Movement by Storms on a Rocky Shore Platform in Laghdira, Northwest Morocco. *Remote Sens.* **2022**, *14*, 4102. [CrossRef]
17. Hoffmeister, D.; Curdt, C.; Bareth, G. Monitoring the sedimentary budget and dislocated boulders in western Greece–results since 2008. *Sedimentology* **2020**, *67*, 1411–1430. [CrossRef]
18. Nagle-McNaughton, T.; Cox, R. Measuring Change Using Quantitative Differencing of Repeat Structure-From-Motion Photogrammetry: The Effect of Storms on Coastal Boulder Deposits. *Remote Sens.* **2020**, *12*, 42. [CrossRef]
19. Pérez-Alberti, A.; Trenhaile, A. Clast mobility within boulder beaches over two winters in Galicia, northwestern Spain. *Geomorphology* **2015**, *248*, 411–426. [CrossRef]
20. Blair, T.C.; McPherson, J.G. Grain-size and textural classification of coarse sedimentary particles. *J. Sediment. Res.* **1999**, *69*, 6–19. [CrossRef]
21. Scerri, S. Sedimentary evolution and resultant geological landscapes. In *Landscapes and Landforms of the Maltese Islands*, 1st ed.; Gauci, R., Schembri, J., Eds.; Springer: Cham, Switzerland, 2019; pp. 31–47.
22. Galdies, C. *The Climate of Malta: Statistics, Trends and Analysis 1951–2010*; National Statistics Office: Valletta, Malta, 2011.
23. Causon Deguara, J. A study of shore deposits on the coastline between Xgħajra and Żonqor—Marsascala. Unpublished Master of Arts Dissertation, Department of Geography, University of Malta, Msida, Malta, 2015.
24. Biolchi, S.; Furlani, S.; Antonioli, F.; Baldassini, N.; Causon Deguara, J.; Devoto, S.; Di Stefano, A.; Evans, J.; Gambin, T.; Gauci, R.; et al. Boulder accumulations related to extreme wave events on the eastern coast of Malta. *Nat. Hazards Earth Syst. Sci.* **2016**, *3*, 5977–6019. [CrossRef]
25. Mottershead, D.; Bray, M.; Soar, P.; Farres, P.J. Extreme wave events in the central Mediterranean: Geomorphic evidence of tsunami on the Maltese Islands. *Z. Geomorphol.* **2014**, *58*, 385–411. [CrossRef]
26. Mottershead, D.; Soar, P.; Bray, M.; Hastewell, L.J. Reconstructing Boulder Deposition Histories: Extreme Wave Signatures on a Complex Rocky Shoreline of Malta. *Geosciences* **2020**, *10*, 400. [CrossRef]
27. Causon Deguara, J.; Gauci, R. Evidence of extreme wave events from boulder deposits on the south-east coast of Malta (Central Mediterranean). *Nat. Hazards* **2017**, *86* (Suppl. 2), 543–568. [CrossRef]
28. Agisoft Metashape User Manual: Professional Edition. 2019. Available online: https://www.agisoft.com/pdf/metashape-pro_1_5_en.pdf (accessed on 1 March 2022).

29. Haala, N.; Rothermel, M. Dense multiple stereo matching of highly overlapping UAV imagery. *ISPRS Arch.* **2012**, *39*, B1. [CrossRef]

30. Autret, R.; Dodet, G.; Fichaut, B.; Suanez, S.; David, L.; Leckler, F.; Ardhuin, F.; Ammannd, J.; Grandjean, P.; Allemande, P.; et al. A comprehensive hydro-geomorphic study of cliff-top storm deposits on Banneg Island during winter 2013–2014. *Mar. Geol.* **2016**, *382*, 37–55. [CrossRef]

31. Scicchitano, G.; Pignatelli, C.; Spampinato, C.R.; Piscitelli, A.; Milella, M.; Monaco, C.; Mastronuzzi, G. Terrestrial laser scanner techniques in the assessment of tsunami impact on the Maddalena peninsula (south-eastern Sicily, Italy). *EPS* **2012**, *64*, 889–903. [CrossRef]

32. Engel, M.; May, S.M. Bonaire's boulder fields revisited: Evidence for Holocene tsunami impact on the Leeward Antilles. *Quat. Sci. Rev.* **2012**, *54*, 126–141. [CrossRef]

33. Hoffmeister, D.; Ntageretzis, K.; Aasen, H.; Curdt, C.; Hadler, H.; Willershäuser, T.; Bareth, G.; Brückner, H.; Vött, A. 3D model-based estimations of volume and mass of high-energy dislocated boulders in coastal areas of Greece by terrestrial laser scanning. *Z. Geomorphol.* **2014**, *58* (Suppl. 3), 115–135. [CrossRef]

34. Mastronuzzi, G.; Pignatelli, C. The boulder berm of Punta Saguerra (Taranto, Italy): A morphological imprint of the Rossano Calabro tsunami of April 24, 1836? *EPS* **2012**, *64*, 829–842. [CrossRef]

35. Biolchi, S.; Denamiel, C.; Devoto, S.; Korbar, T.; Macovaz, V.; Scicchitano, G.; Vilibić, I.; Furlani, S. Impact of the October 2018 storm Vaia on Coastal Boulders in the Northern Adriatic Sea. *Water* **2019**, *11*, 2229. [CrossRef]

36. Biolchi, S.; Furlani, S.; Devoto, S.; Scicchitano, G.; Korbar, T.; Vilibic, I.; Sepic, J. The origin and dynamics of coastal boulders in a semi-enclosed shallow basin: A northern Adriatic case study. *Mar. Geol.* **2019**, *411*, 62–77. [CrossRef]

37. Scicchitano, G.; Scardino, G.; Tarascio, S.; Monaco, C.; Barracane, G.; Locuratolo, G.; Milella, M.; Piscitelli, A.; Mazza, G.; Mastronuzzi, G. The First Video Witness of Coastal Boulder Displacements Recorded during the Impact of Medicane "Zorbas" on Southeastern Sicily. *Water* **2020**, *12*, 1497. [CrossRef]

38. Gienko, G.A.; Terry, J.P. Three-dimensional modeling of coastal boulders using multi-view image measurements. *Earth Surf. Processes Landf.* **2014**, *38*, 853–864. [CrossRef]

39. Lane, S. Slow science, the geographical expedition, and Critical Physical Geography. *TCG* **2017**, *61*, 84–101. [CrossRef]